# Three-dimensional geological modelling of AEM resistivity data — A comparison of three methods

A.-S. Høyer [a,*], F. Jørgensen [a], N. Foged [b], X. He [a], A.V. Christiansen [b]

[a] Geological Survey of Denmark and Greenland, GEUS, Denmark
[b] HydroGeophysics Group, Department of Geoscience, Aarhus University, Denmark

## ABSTRACT

Spatially dense Airborne Electromagnetic Method (AEM) surveys are increasingly acquired to provide a background for creating 3D geological models. These datasets provide a high degree of detail that is very time-consuming and challenging to incorporate in manually-produced geological models. Automated modelling methods are therefore needed to make the modelling process more time-efficient. In this study we evaluate the results of two automated modelling methods against the results of a manually constructed geological model. The study area is characterized by a sequence of Quaternary glacial till deposits on top of Pre-Quaternary sand and clay deposits. The tested automatic methods are 1) an approach for clay fraction modelling, where borehole and AEM resistivity models are integrated through inversion, and 2) a stochastic approach based on transition probability indicator statistics. The most significant difference between the model results is the ability of the manually constructed geological model to contain stratigraphic information, contrary to the sand–clay models generated by the automated approaches. When all the model results are translated to binary models, they are generally in good agreement. The models have different strengths and limitations and the later application of the model should therefore be taken into consideration when choosing the modelling approach.

© 2015 The Authors. Published by Elsevier B.V. This is an open access article under the CC BY-NC-ND license (http://creativecommons.org/licenses/by-nc-nd/4.0/).

## Contents

* Corresponding author.
   *E-mail address:* ahc@geus.dk (A.-S. Høyer).

## 1. Introduction

At the Geological Survey of Denmark and Greenland (GEUS) we work in complex glacial settings, in which it can be difficult or even impossible to correlate between boreholes without additional information (Høyer et al., 2013). Geological models in Denmark are therefore typically based on datasets consisting of both boreholes and geophysical data. Particularly the Airborne Electromagnetic Method (AEM) has been extensively used (Møller et al., 2009), and at this moment, about a third of the country is covered with AEM surveys (Siemon et al., 2009). The interpretation of the large AEM surveys is highly time-consuming, and it is therefore important to develop more time-efficient approaches for transforming the resistivity information into geological or hydrological models (Foged et al., 2014; Gunnink et al., 2012; Koch et al., 2014). In this study, we compare three different modelling methods: manually constructed knowledge-driven geological modelling (MCG), clay fraction modelling (CF) and stochastic simulations conducted in the Transition Probability Geostatistical Software (TProGS) (Carle, 1999; Carle and Fogg, 1996).

The MCG method is based on a knowledge-driven method, where the modeller integrates as much information as possible and utilises knowledge of regional stratigraphy, geological processes, etc. This results in *one* model that represents *the geologist's best estimation* of the geological setting (Jørgensen et al., 2013; Kessler et al., 2009; Royse, 2010; Wycisk et al., 2009). Traditionally, the outcome is a 'layer-cake' model, where layer units are bounded by stratigraphic interfaces (Turner, 2006). Recently, however, a concept for voxel modelling has been proposed by Jørgensen et al. (2013), which is particularly useful in areas with spatially dense AEM surveys.

A fast, but imprecise geological model can be obtained through a direct translation of resistivities to lithology. However, since resistivity intervals for different sediments overlap, background knowledge or information from other sources is necessary for the lithologies to be distinguished properly. Furthermore, the simple translation does not take account for a series of limitations, e.g. resolution capability, depth of penetration, variations in groundwater salinity and the degree of saturation (Jørgensen et al., 2013). In order to obtain a better translation from resistivity to lithology, Christiansen et al. (2014) and Foged et al. (2014) have developed the *CF modelling* method. Here, an inversion approach is used to find the optimum translation function between resistivity and the relative amount of lithological clay in borehole logs expressed as the clay fraction. The translator function is allowed to change to allow for spatial variations.

The geostatistical methods enable the computation of *a number of equally plausible realisations* of the geological setting under a given set of conditions and assumptions. This has proved to be relevant in relation to numerical groundwater modelling and research. Among the most common geostatistical methods are multiple-point statistical methods (Strebelle, 2002) and the transition probability-based methods (Carle and Fogg, 1996). In this study, we operate with the geostatistical software TProGS, which is based on a two-point geostatistical method that uses transition probabilities to describe the rate of changes of geological facies in space (Carle, 1999). The software enables conditional data to be incorporated in the stochastic simulation process, in such a way that the random process honours the data at specific locations (e.g. Lee et al., 2007). Geophysical data such as ground penetrating radar and seismic data have often been utilised in stochastic simulations (De Benedetto et al., 2012; Engdahl et al., 2010), but to our knowledge, AEM data have only been used in a few studies (Gunnink and Siemon, 2014; He et al., 2014a, 2014b).

Many geological surveys have started to present their geological knowledge through 3D geological models as an alternative to traditional geological maps (Berg et al., 2011; Kessler et al., 2009; Stafleu et al., 2011). Some of the surveys, like the Geological Survey of the Netherlands (Van der Meulen et al., 2013) and the British Geological Survey (Kessler et al., 2009), are generating nationwide geological models, and in Denmark,

we are at the moment of developing a strategy for a future national geological model. The current study is a part of the research in geological modelling applications. Here, we evaluate the three different modelling methods based on results from a study area in a sedimentary geological environment that has been mapped with high-resolution AEM (Schamper et al., 2014). In the following, we will, by comparing to the MCG model, evaluate the ability of the automated methods to resolve the geology and to provide realistic geological structures.

## 2. Regional geology

The study area is located in the eastern part of Jutland, Denmark, and covers an area of 156 km$^2$ (Fig. 1). In this part of the country, the aquifers are located above marine, very fine-grained, impermeable marls and clays that were deposited during mid-late Eocene (Larsen and Sand-Jensen, 2006). The very fine-grained deposits are overlain by marine Oligocene sediments consisting of clay and silty clay (Rasmussen et al., 2010). During the Miocene, a more coastal environment dominated and delta lobes transgressed from NNE towards SSW across Jutland. This resulted in interlayered marine clays and deltaic deposits in the form of fine- to coarse-grained sand deposited in a pro-delta environment (Rasmussen et al., 2010). According to the stratigraphic overview of the delta lobes in Jutland, the clay deposits in the study area belong to the Vejle Fjord Formation, whereas the sand deposits belong to the Billund Formation (Rasmussen et al., 2010). The stratigraphy and depositional environments are described in detail by Rasmussen et al. (2010).

The area was covered by ice sheets numerous times during the Quaternary. The glaciers transgressed the study area from different directions, some from the south-east through the Baltic depression, and others from the north and north-east (Houmark-Nielsen, 2011). The majority of the Quaternary sediments are of glacial and glacifluvial origin, but glaciolacustrine and meltwater sediments are also common. The Quaternary deposits are usually heterogeneous on both small- and large scales. Large-scale glacial structures include buried valleys (Jørgensen and Sandersen, 2006) and glaciotectonic structures (e.g. Houmark-Nielsen, 1983; Houmark-Nielsen and Berthelsen, 1981; Pedersen and Petersen, 1997).

## 3. Data

### 3.1. SkyTEM101 survey

The main dataset in this study is a large airborne electromagnetic dataset (Fig. 1) acquired in the framework of the NiCA research project in 2011 (Refsgaard et al., 2014), using a high resolution version of the SkyTEM system (Sørensen and Auken, 2004) called the SkyTEM101 system (Schamper et al., 2014). The SkyTEM101 system was developed with the objective to increase the resolution of the top 30 m. Schamper et al. (2014) evaluated the SkyTEM101 results against boreholes and found a good fit for more than 75% of the boreholes. The SkyTEM101 system has a small transmitter loop from which it operates with two moments: a super-low moment (SLM) of 910 A m$^2$ and a high moment (HM) of 7150 A m$^2$. As a consequence of a very short turn-off time of the SLM, it is possible to use data at very early times (5–6 μs from begin of ramp). According to Schamper et al. (2014), the best lateral resolution of the top 30 m is estimated to be in the order of 30–40 m, whereas the depth of investigation is around 100 m. The SkyTEM survey covers 2000 line km with an in-line sounding spacing of about 15 m, resulting in more than 100,000 soundings. The survey has been flown with three different line spacings: in the eastern part the nominal line spacing is 100 m; in the western part it is 50 m; and in a smaller area west of the town Odder, cross-lines have been flown with a nominal line spacing of 50 m (Fig. 1).

The data have been processed according to the recommended approach by Schamper et al. (2012), which is a modified version of the processing approach for normal SkyTEM data described by Auken
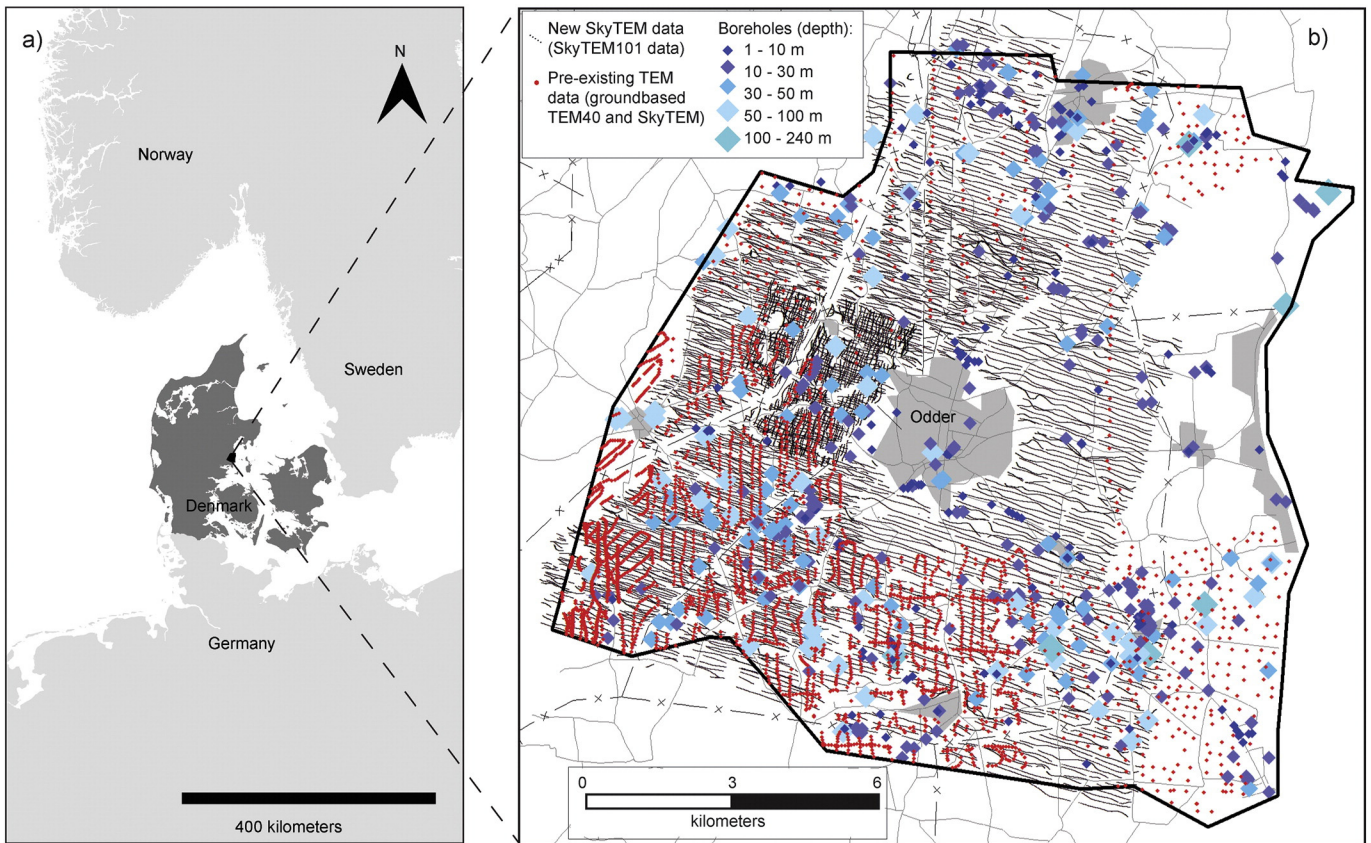
Fig. 1. a: Location of the study area. b: Data in the study area.

et al. (2009). Processing and inversion of the survey are described in detail in Schamper et al. (2014). One of the important steps in the processing is manual inspection and removal of data that are affected by couplings to man-made installations. The data inversion is based on a local, 1D forward response, and to obtain pseudo-3D volumes, the models are mutually interconnected along and between flight-lines (Viezzoli et al., 2008). The inversion was performed as a multi-layer inversion with 29 layers where thicknesses increased logarithmically downwards. During the modelling and in the presentation, the data are displayed as a 3D volume that is constructed from stacked 2D grids, and cover the elevation range from −70 m to the surface. The grid cells are 50 m by 50 m laterally and 2 m vertically.

### 3.2. Pre-existing TEM data

In parts of the study area, pre-existing SkyTEM data was available prior to the NiCA project (Fig. 1). These data were acquired during different groundwater mapping campaigns in the mid 2000's using settings typical for that time. The older SkyTEM data have a higher moment and a larger depth of investigation than the SkyTEM101 data, but are less focused on the shallowest parts (Sørensen and Auken, 2004). Ground based TEM soundings were also available in the study area. These were acquired in different mapping campaigns during the 1990's, and a total of more than 500 ground based TEM soundings are present within the study area (Fig. 1). The soundings were collected with the Geonics PROTEM47 instrument using a 40 m by 40 m central loop configuration giving a depth of investigation of 80–150 m, depending on the geology and the noise level.

### 3.3. Boreholes

Within the study area, data from around 700 boreholes are available in the national Danish borehole database, Jupiter (Møller et al., 2009)

(Fig. 1). The database contains information on the drilling method, purpose, geographical coordinates, depth, drill logs, borehole sample descriptions, layer boundaries, groundwater head, and many other items. The majority of the boreholes were drilled for groundwater abstraction, but a considerable number were carried out for geotechnical, raw material and waste site examination. A few boreholes have been investigated palynologically (Dybkjær, 2011a,b) to use them as stratigraphic boreholes in the modelling of Miocene sequence in Jutland (Rasmussen et al., 2010).

Just as the resolution capabilities of the AEM data are considered during modelling, the uncertainty of the borehole information should also be considered. We have therefore quality-rated the boreholes according to the approach described by He et al. (2014a). The boreholes were divided into five groups, from good to poor quality where the fifth group represents boreholes without usable information. The borehole ratings for the study area are summarised in Table 1.

## 4. Conceptual geological model

Initially, a conceptual geological model was constructed for the entire area (Fig. 2). The model volume was subdivided mainly based on the geological origin. This subdivision was utilised to define a study area for the geological modelling exercises. The model was based on all available data (Fig. 1) and pre-existing geological and stratigraphical knowledge. The final model contains six main units (Fig. 2):

A. The Palaeogene unit
B. The Miocene unit
C. The Boulstrup tunnel valley
D. A thin glacial unit
E. A thick glacial unit
F. The glaciotectonic complex.

**Table 1**
Rating of borehole data quality in Unit (E). Modified from He et al. (2014a).

| Quality group | No. of boreholes (percentage) | Short description |
|---|---|---|
| 1 | 25 (14%) | High data sampling frequency, coordinates and level measured with differential GPS, trusted contractor and high-quality drilling method |
| 2 | 34 (19%) | Typically normal sampling frequency, trusted contractor and drilling method but without differential GPS measurements |
| 3 | 43 (24%) | Typically normal sampling frequency, poor drilling method and samples |
| 4 | 10 (6%) | Low data sampling frequency, very poor drilling method and samples |
| 5 | 65 (37%) | Very low quality, no data |

In this study, we have modelled the area, where Unit E is present (Fig. 2), but the outline was slightly modified to accommodate hydrostratigraphic considerations (marked with blue in Fig. 2). The units within the modelled area (Units A, B and E) are briefly described in the following.

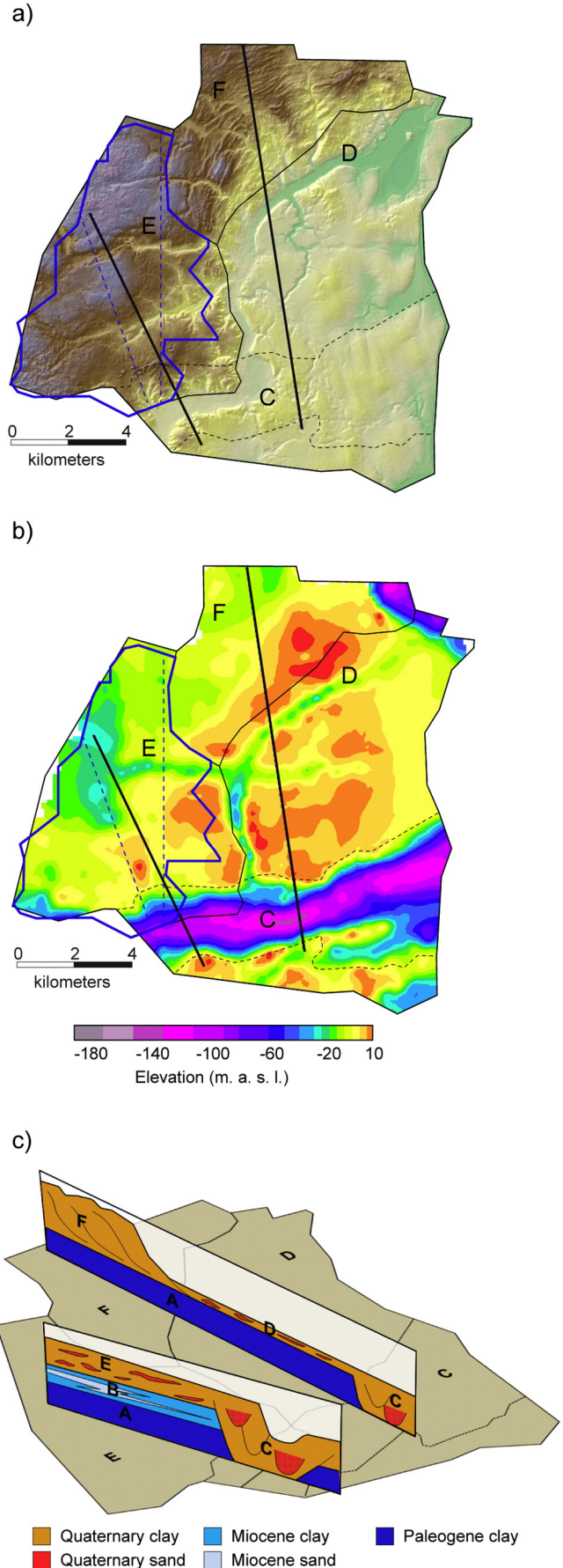### 4.1. The Palaeogene unit (Unit A)

Borehole descriptions from boreholes that reach the Palaeogene show that it is mainly composed of the marine Lillebælt Clay and Søvind Marl Formations (Heilmann-Clausen et al., 1985). These clays and marls are extremely fine-grained with a high content of smectite, giving them a high electrical conductivity. They are therefore easily recognised both in the borehole data, owing to their plastic appearance, and in the resistivity data where they show very low resistivities (less than 5–7 Ω-m). The surface of the Palaeogene is incised by both deep and shallow valleys (Fig. 2b). The elevation of the surface ranges from about 140 m below sea level to about 15 m above sea level.

### 4.2. The Miocene unit (Unit B)

The Miocene unit is composed of the Billund and Vejle Fjord Formations (Rasmussen et al., 2010). The Brejning Formation is also included in the Miocene unit although it is partly of Upper Oligocene age. The lower part of this unit is mainly composed of silty clay (Brejning Formation), whereas the upper part is composed of silty clay, silt and sand (Vejle Fjord Formation) interbedded with deltaic sandy deposits (Billund Formation). Generally, the lower part is more electrically conductive than the upper, sandier part. There is no distinct resistivity boundary between the Miocene unit and Unit E since the lower part of Unit E also is sandy in most places. The boundary is therefore typically deduced from borehole information. The modelled surface of the Miocene unit is smooth with only little variation and its elevation ranges from 18 to 52 m above sea level. Minor details in the shape that indicate meltwater erosion and glacial deformation are not included in the surface. The thickness of the unit is generally between 30 and 60 m.

### 4.3. The thick glacial unit (Unit E)

The thick glacial unit is found in the western part of the area (Fig. 2). It directly overlies the Miocene Unit except towards the south where it

a)

b)

-180   -140   -100   -60   -20   10
Elevation (m. a. s. l.)

c)

Quaternary clay    Miocene clay    Paleogene clay
Quaternary sand    Miocene sand

**Fig. 2.** The conceptual geological model illustrated in three figures. The 2D figures (a and b) are shown together with the delineation of the units and the locations of the conceptual cross sections (c). The blue line delineates the focus area, which is slightly modified from the outline of unit E due to hydrostratigraphic issues. The two dashed blue lines indicate the position of the two profiles shown in Figs. 5–7. (a) Topography of the area. (b) Visualization of the Top Palaeogene surface. (c) Conceptual cross-sections through the area. (For interpretation of the references to color in this figure legend, the reader is referred to the web version of this article.)

overlies the Boulstrup tunnel valley. It is laterally bounded by the glaciotectonic complex (Unit F) towards the northeast. Towards south and east it pinches out due to surface erosion. It is composed of a mixture of glacial sediments, varying from coarse meltwater sediments to clay till and glaciolacustrine silt and clay. The sequence is occasionally deformed, and rafts of Miocene and Palaeogene clay are sporadically found within the sequence. The thickness of the unit is typically between 20 and 50 m. The surface expression varies, but it is generally undulating with a number of erosional valleys with small streams. Indications of glaciotectonic deformation are seen locally, and hummocky topography indicates ice wastage elsewhere.

## 5. Manually constructed geological model (MCG)

The MCG model covers both the Pre-Quaternary (Units A and B) and the Quaternary (Unit E) deposits in the study area. A 3D view of the model results is shown in Fig. 3. The model is constructed as a voxel model in the software package Geoscene3D (I-GIS, 2014). The modelling grid was chosen to be 50 m by 50 m laterally and 2 m vertically. These dimensions were selected to enable incorporation of detailed geological heterogeneities, while securing the modelling efficiency.

During the modelling, uncertainty related to both the borehole and the geophysical data are taken into consideration. Thus, the ratings of the boreholes are considered together with the entire borehole descriptions. Trustworthy borehole information gives valuable point-information, but in the Quaternary part where the deposits are highly heterogeneous, it can be difficult to extrapolate the information from the boreholes. The depth to which the TEM data penetrate is visualised as the DOI (depth of investigation) while modelling. The resolution capability of the TEM data is also considered, such that the resistivity information generally is trusted more at shallow depths, where the resolution capabilities are best. At great depths, the larger footprint of
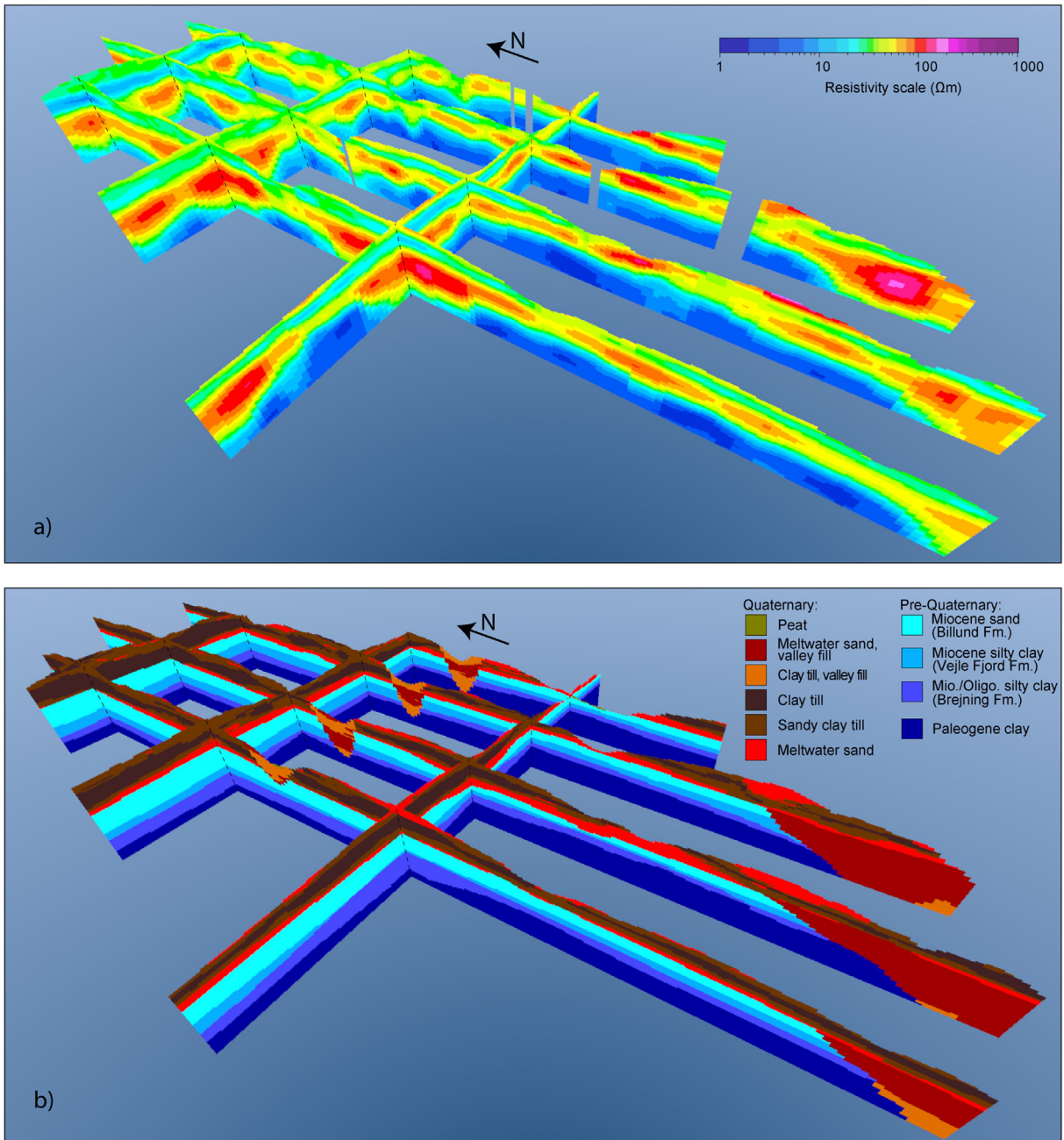


**Fig. 3.** Slices through a) the resistivity grid and b) the MCG model results. Vertical exaggeration = 6×.

the TEM method makes it impossible to resolve small details, but the method is superior in mapping the depth to good conductors also at great depths (Jørgensen et al., 2003). This part of the information is therefore highly trusted.

The Pre-Quaternary part of the model (Units A and B) is initially constructed as a layer-based model, whereupon voxels between the layers are populated with lithology. This strategy was chosen because the Pre-Quaternary geology is relatively homogeneous. The modelled units constitute the Palaeogene, the Brejning Fm., the Vejle Fjord Fm. and the Billund Fm. Modelling of the Palaeogene surface was largely based on the elevation of the good electrical conductor. This was derived from the pre-existing TEM and SkyTEM data that generally have a better DOI than the new SkyTEM101 data. The borehole information played a vital role for modelling the three lithological formations in the Miocene sequence. Thus, the surface of the Brejning Fm. was largely modelled from stratigraphic boreholes, which were investigated palynologically (Dybkjær, 2011a,b). Unfortunately, information concerning this boundary is in general difficult to extract from more conventional boreholes, since the driller's descriptions of the Brejning Fm. and the overlying Vejle Fjord Fm. are commonly very similar. Due to sparse borehole data, the surface of the Brejning Fm. is therefore considered highly uncertain. The surfaces of the Vejle Fjord Fm. and the Billund Fm. were also modelled mainly on the basis of borehole information, and partly on the basis of the TEM resistivities.

The Quaternary part (Unit E) was modelled using the voxel modelling tools described in Jørgensen et al. (2013). The modelled categories were defined on the basis of the most common lithologies witnessed in the boreholes (sandy clay till, clay till, peat, and meltwater sand in and outside the buried valleys). Surfaces to define the overall units were constructed in the first step of the modelling process. In the second step, the surfaces were used as boundaries for the lithological population of the voxel model grid. Thirdly, the 3D grid was adjusted by manual voxel editing by adding details, as the sand lenses within the clay till deposit. These sand lenses were described in the boreholes, but they are often too small to be fully resolved in the SkyTEM data. Between the boreholes, the sand lenses were therefore incorporated in the model, where the SkyTEM resistivities show small changes towards higher values.

## 6. Clay fraction (CF) model

The clay fraction (CF) model covers the entire study area in Fig. 2a, but here we focus at the model results from the western part of the area. The complete CF-setup is specified in detail in Foged et al. (2014). The CF results are displayed with a discrete colour scale showing percentages of clay in 10% intervals. The final CF-model was compiled with a horizontal discretization of 50 by 50 m, and a vertical discretization of 4 m from surface to sea level and 8 m below this. The change in vertical discretization at sea level was chosen in order to reflect the decreasing resolution with depth in the underlying resistivity model. The basis for the CF inversion is the clay fraction calculated from the resistivity models ($CF_{res}$) and the observed clay fraction in the lithological logs from boreholes ($CF_{log}$). The quality of borehole samples vary a lot and these might therefore be associated with much uncertainty. Nevertheless, it is normally easy for the driller and/or geologist who described the borehole samples, to distinguish between clay and non-clay deposits. The AEM results are also sensitive to this distinction, which is why these two groups are used.

The clay fractions from the resistivity logs and lithological logs are derived in the following way: initially, the $CF_{log}$ values are calculated for each borehole in a number of elevation intervals, by summarising the thickness of the clay units in each interval and dividing them with the length of the interval. Secondly, a starting model is defined for a translator function that is used to calculate the $CF_{res}$ values. This translator function is used to assign a weight for each resistivity layer within the considered calculation interval. Low resistivities will get a weight

close to 1 corresponding to clay; high resistivities a weight close to 0 corresponding to non-clay; and intermediate resistivities are weighted between 0 and 1. For example, imagine a layer of 30 Ω-m which we say has a weight of 0.8. If this layer covers 3 m of a given interval, the actual clay contribution from that layer will be only 2.4 m due to the weight (3 ∗ 0.8). As for the borehole values, the $CF_{res}$ values are calculated for each sounding position in all intervals by summarising the weighted clay thicknesses and dividing them with the length of the interval. These values are then interpolated to the borehole positions with a kriging routine for comparison with the observed $CF_{log}$ values. The translator function can vary both horizontally and vertically.

In the study area, the translator function is specified in a regular 3D grid, with a horizontal discretization of 1 km. In order to migrate information from regions with high borehole density to areas with sparse information, constraints have been applied between the translator functions in the 3D translator function grid. These constraints have also been applied to stabilize the inversion and avoid abrupt and unrealistic changes in the translator function from node to node. In an iterative inversion process the parameters of the translator functions are updated to minimize the difference between the $CF_{res}$ and the $CF_{log}$ values. Finally, the optimised and spatially distributed translator functions are utilised to transform the resistivity values in the sounding positions to clay fractions, and kriging is finally used to take these discrete points into a regular 3D CF model. Uncertainty of the input resistivity models and the borehole logs (based on the borehole rating, Table 1) are taken into account in the inversion scheme, as discussed in Foged et al. (2014). The final CF model provides an estimate of the relative clay content (clay fraction). In the CF approach, the term *clay* covers all the various clay types (clay till, meltwater clay, Pre-Quaternary clay, etc.). The non-clay deposits are denoted 'sand', because this is the major non-clay element in the area. In practice, this group covers all non-clay deposits including for instance peat, but according to the lithological borehole logs, the vast majority show either clay (55%) or sand/gravel (41.6%).

## 7. Stochastic (TRroGS) model

The geostatistical software TProGS (Carle, 1999) was used to generate 10 geological simulations within the thick glacial unit (Fig. 2, area E). The modelling approach has been described in detail by He et al. (2014a). The simulation grid was chosen to be 20 by 20 m laterally and 2 m vertically.

In order to use the AEM data in the stochastic simulations, the resistivity data need to be converted to lithological categories. In He et al. (2014a) a procedure was therefore developed to translate the resistivities from the AEM data into the two simulated categories: sand or clay. The relationship between the probability of a certain lithology and the resistivity was expressed by using a histogram probability matching method. Initially, the borehole data were converted from detailed geological descriptions to a binary system of sand and clay. In this regard, peat deposits were considered as clay deposits, contrary to the CF method. The discretization of borehole data was done for fixed vertical steps of 5 cm. The categorical data for each vertical interval were then paired with resistivity data from the surrounding TEM soundings. A bar histogram was created, illustrating the percentage of sand and clay within bin lengths of 10 Ω m. Finally, a curve fitting algorithm was performed on the histogram bars. The probability of the category is then read from the fitted curve for any given resistivity value in the AEM dataset.

The histogram was used as a tool to define a cut-off value for the resistivity level that distinguishes clay and sand, which is a pre-requisite for incorporating the AEM data in the simulations. The cut-off value was found in He et al. (2014a) by reading the resistivity value at 50% sand probability. This resulted in 55 Ω m, which however, gave an unrealistic sand proportion calculated for the AEM data (12%) compared to the sand proportion in the boreholes (29%). This mismatch was probably a consequence of an uneven distribution of the boreholes in the

study area. In order to avoid this effect, an empirical cost function was used to obtain an optimal sand proportion (He et al., 2014a). This resulted in a cut-off value of 46 Ω m, giving a calculated sand proportion from the AEM data of 23%.

The geostatistical software TProGS consists of three main steps. Firstly, the transition probabilities are established from the chosen data. In this study, the spatially dense AEM data were used to evaluate the transition probabilities in the horizontal direction, whereas the detailed point information from the boreholes was used as input for the vertical transition probabilities. Secondly, in TProGS, Markov Chain models are developed in order to represent the spatial variability. In this study, the embedded Markov Chain model was developed by using the observed transition probabilities, where clay was used as the background facies. The observation data suggested a sand proportion of 23%, and the sand lenses measured 5 m vertically and 500 m horizontally. Finally, the stochastic simulations were carried out using conditional sequential indicator simulation and quenching. In the simulations the sand and clay categories derived from the resistivity data were used as soft data by

considering the actual resistivity value at each position. In this way, a very high resistivity as 80 Ω-m receives a larger probability for sand in the soft conditioning than a resistivity value of 50 Ω-m, even though both values are above the cut-off value (46 Ω-m). In principle, the probability of each category can be up to 100%, but in reality the highest probability reaches 87%. Soft conditioning was also used for the boreholes, where the conditioning was based on the evaluated uncertainty. Thus, the boreholes in the best quality group were used as hard conditioning data, whereas the other groups were ascribed a certainty ranging from 95% for group 2 to 85% for group 4. The borehole data are therefore generally harder conditioned than the AEM data.
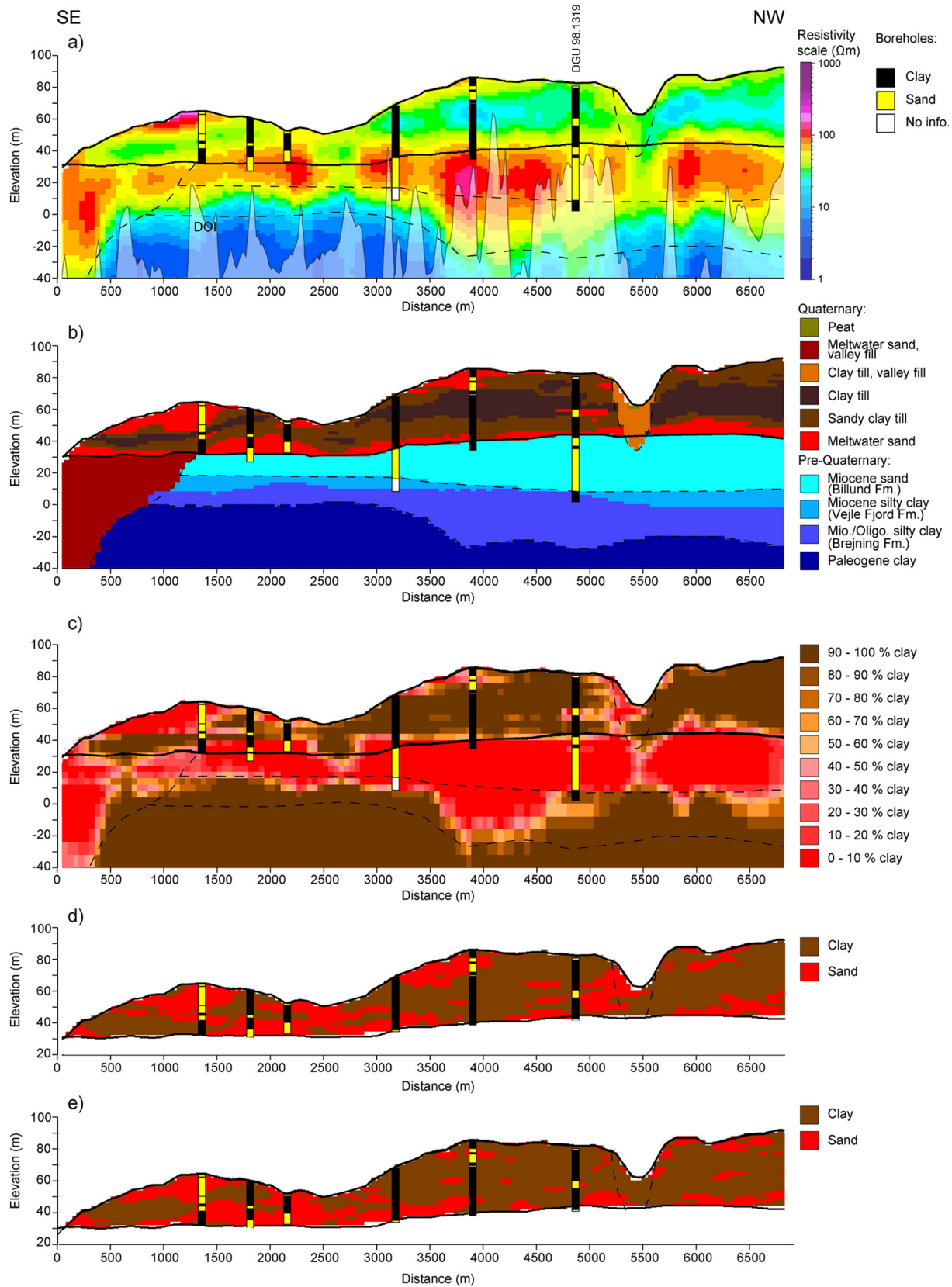
## 8. Comparison of the model results

### 8.1. Visual inspection

For the Pre-Quaternary part, we only have results from the MCG model (Figs. 4c, 5b and 6b) and the CF model (Figs. 4d, 5c and 6c). The
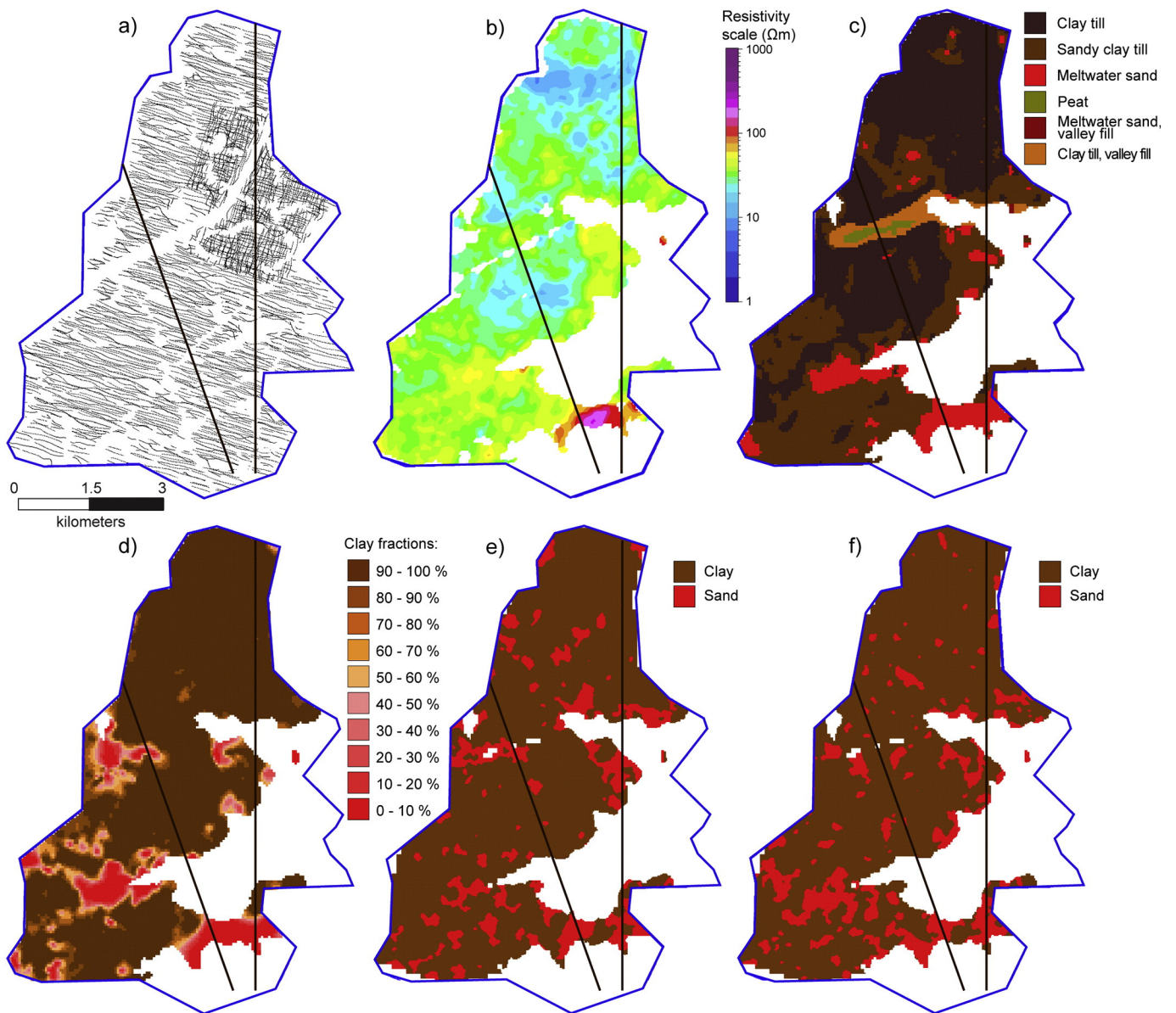


**Fig. 4.** Horizontal slices through the area. a) Position of the SkyTEM soundings together with the locations of the profiles in Figs. 5 and 6. b–f) Horizontal slice at elevation 61 m, shown with b) the resistivity grid, c) the MCG model results, d) the CF model results, e) TProGS simulation no. 1 and f) TProGS simulation no. 2. The blank area to the east is due to lower topography here.

Fig. 5. a–e. NW–SE profile shown with the resistivity grid and the model results (for location of the profile see Fig. 4). Vertical exaggeration = 15×. Boreholes within a buffer of 100 m of the profile are shown in all the sections. The location of the stratigraphic borehole (DGU 98.1319) is marked. The bottom of the Quaternary (Unit E), is shown as a thick line in all the sections. In a–c the bottom of the valleys, the bottom of the Billund sand and the Top Palaeogene are marked with dashed lines. a) Resistivity grid. The colours are faded below the gridded DOI (depth of investigation). b) The MCG model results from which the dashed boundaries are derived. c) Result of the CF modelling. d) One of the TProGS simulations ("no. 1"). e) Another TProGS simulation ("no. 2"). The TProGS simulations are only conducted for the thick glacial unit, so in d and e the simulations and the borehole information are only shown for this part. (For interpretation of the references to color in this figure legend, the reader is referred to the web version of this article.)
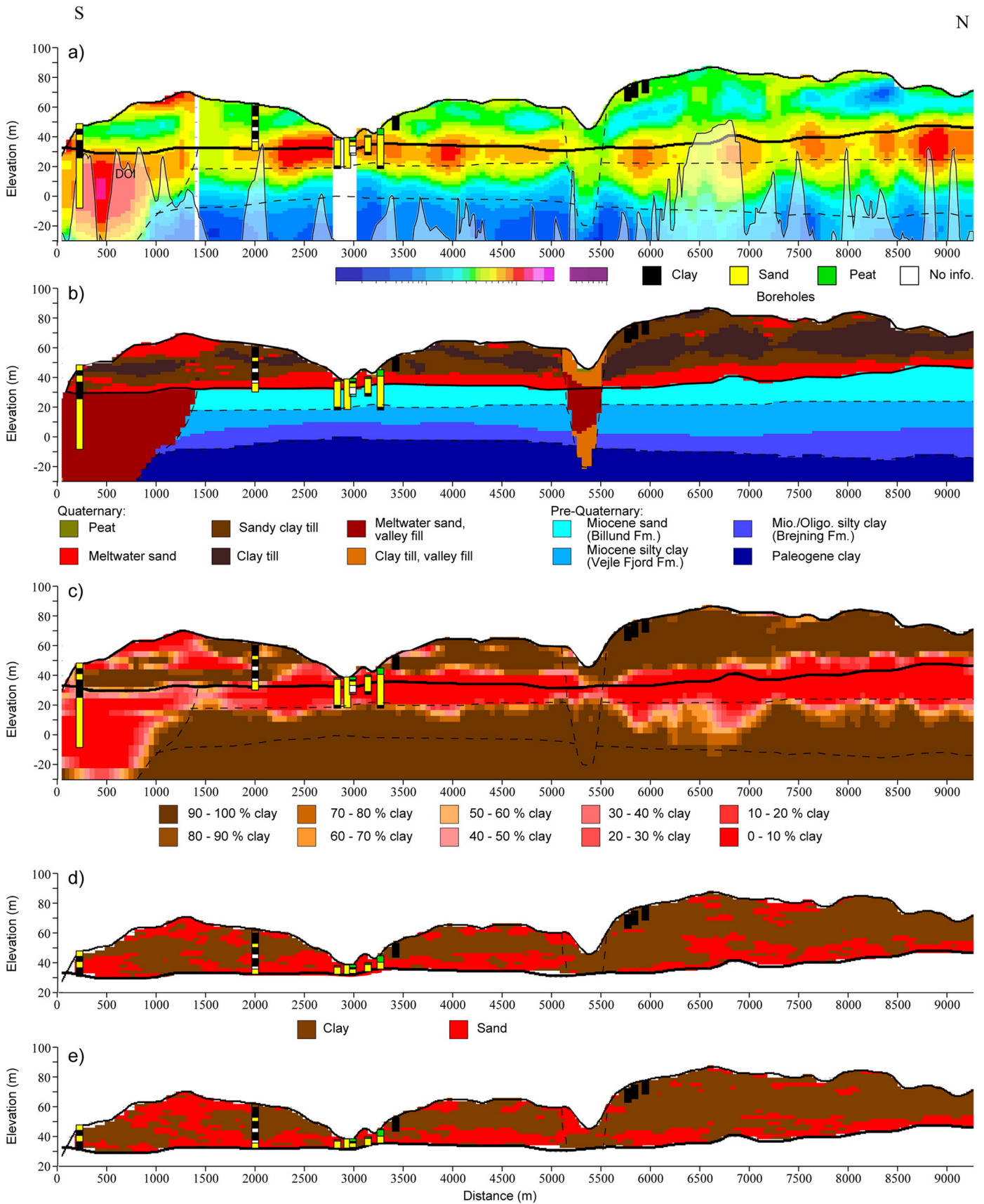
**Fig. 6.** N–S profile shown with the resistivity grid and the model results (for position of the profile see Fig. 4). Vertical exaggeration = 15×. Boreholes within a buffer of 100 m of the profile are shown in all the sections. The bottom of the Quaternary (Unit E), is shown as a thick line in all the sections. In a–c the bottom of the valleys and the Billund sand unit, as well as the Top Palaeogene, are marked with dashed lines. a) Resistivity grid. The colours are faded below the gridded DOI. b) The MCG model results from which dashed boundaries are derived. c) Result of the CF modelling. d) One of the TProGS simulations ("no. 1"). e) Another TProGS simulation ("no. 2"). (For interpretation of the references to color in this figure legend, the reader is referred to the web version of this article.)

MCG model shows a smoothly varied, layered sequence with little heterogeneity, whereas the CF model shows a more variable sequence, mimicking the structures in the resistivity grid. Borehole information becomes very sparse and the resolution capability of the TEM data decreases with depth. The scarcity of borehole information means that the final CF model with depth is increasingly controlled by the resistivity information and the user defined starting model. Contrary to this, it is at these depths that the MCG model shows the largest divergence from the resistivity grid, because the modeller is aware of the decreased resolution capability of the TEM information. Here, the geological modelling is therefore mainly based on the borehole information and geological background knowledge. Consequently, the most distinct differences between the model results appear in those areas, where the SkyTEM resistivity data have low resolution capabilities (e.g. Fig. 5, distance 3500–5000 m).

The CF model shows a relatively sharp but undulating boundary between the upper clay-free deposits and the deeper clayey part (Figs. 5c

and 6c). When compared to the geological model, this boundary is typically situated between the bottom of the Billund sand Fm. and the top of the Palaeogene. The difference is pronounced in Fig. 5c (distance 3500 to 4500 m), where the CF model shows a thick (approximately 20 m) sequence of sand deposits in the interval, where the MCG model shows Miocene silty clay belonging to the Brejning Fm. The undulating appearance of the sand–clay boundary in the CF model is probably due to facies variations within the Brejning Fm. Both the Brejning Fm. and the Vejle Fjord Fm. are described as clayey formations with relatively high and varying silt contents. Areas with high contents of silt typically show high resistivities, and the CF model will therefore typically show sandy deposits here.

Another location that shows sandy deposits at great depths is in the southern part of the profiles (Figs. 5c and 6c, distance 0–1200 m). Here, both the MCG and the CF models show sandy deposits in the area that according to the MCG corresponds to a buried valley. While this buried valley is modelled by both methods, the smaller buried valley (Figs. 5b
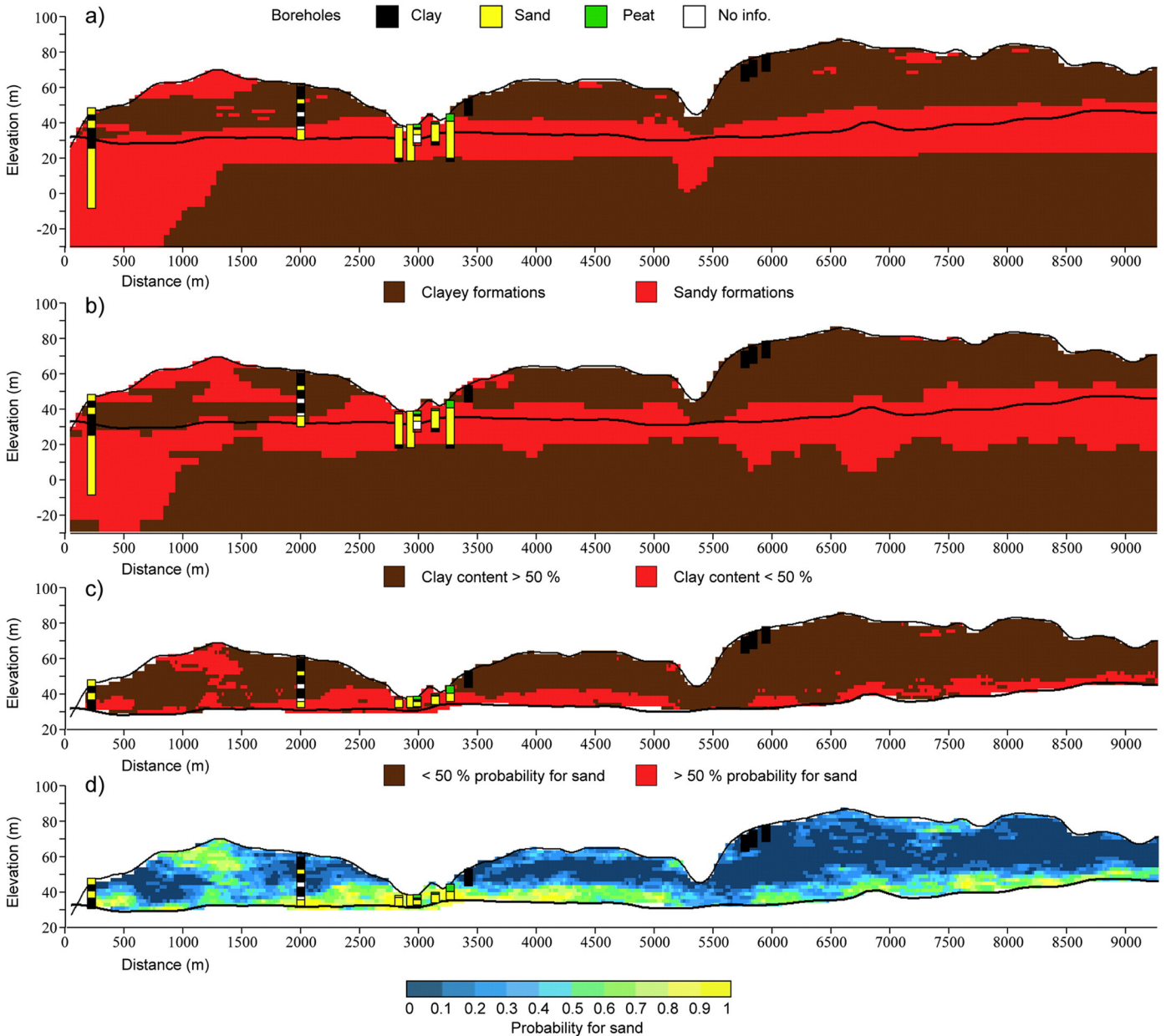


Fig. 7. The same profile as in Fig. 6, where all the model results are divided into two facies: sand and clay: a) the MCG model divided into sand and clay formations, b) the CF model divided into categories representing more and less than 50% clay, c) a probability section derived from the 10 TProGS simulations divided into categories with more and less than 50% probability of sand and d) the probability of sand based on the 10 simulations.

and 6b, distance 5200–5500 m) is only completely captured by the MCG model. The resistivity data was used for modelling this valley but supporting background knowledge such that buried valleys tend to occur below modern valleys (Jørgensen and Sandersen, 2006) was also taken into account. The buried valley is only evident in the resistivity data by slight changes, and the valley is therefore not captured by any of the two automatic modelling methods.
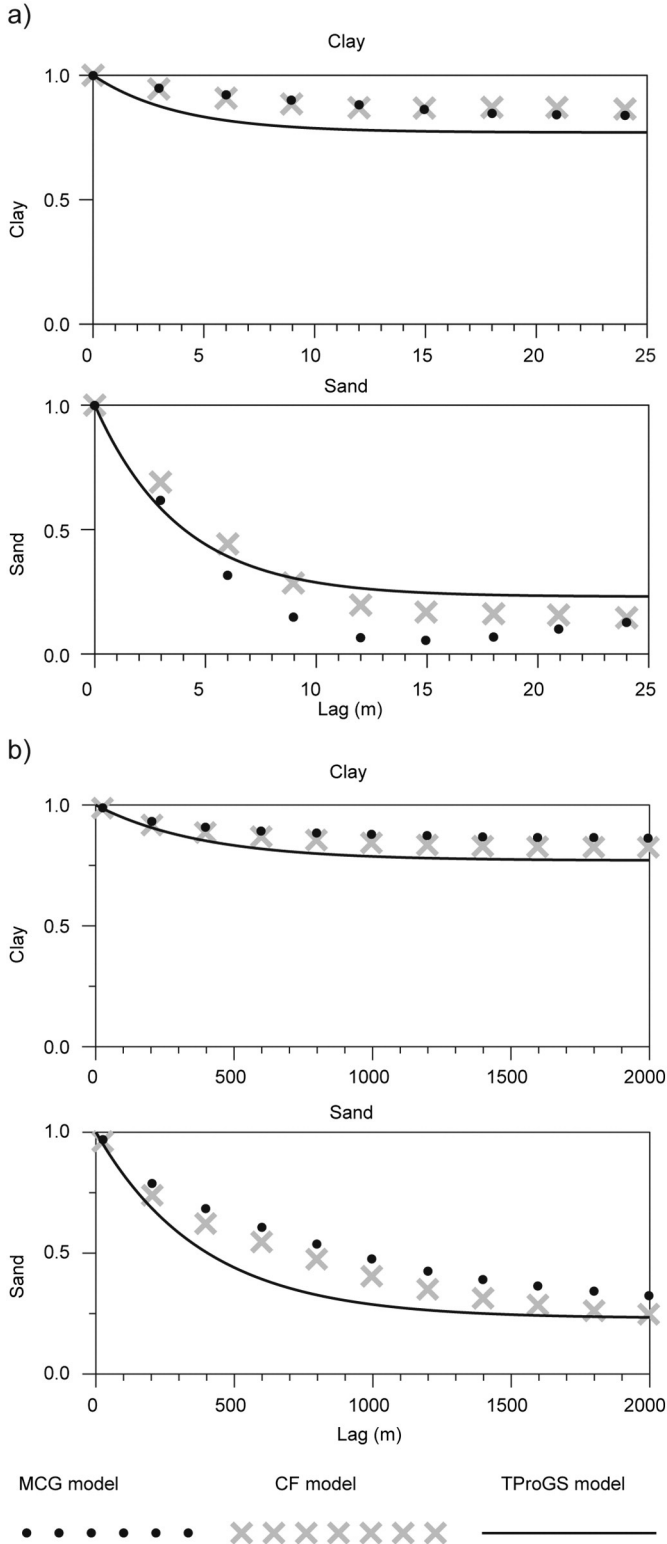


Fig. 8. Transition probabilities for the 3D model grids, shown in a) the vertical and b) the horizontal directions for clay to clay and sand to sand.

In the Quaternary part of the setting, the MCG model distinguishes between clay till and sandy clay till, primarily based on the resistivities but also supported by the borehole descriptions. Since clay is the primary component in both units, they are not discriminated in the binary models (Fig. 5b, c and d). All of the models show a clayey deposit with sand inclusions on top of a more sandy sequence (below 40 m above sea level, Figs. 5–6). The sand lenses in the TProGS model keep almost the same dimensions throughout the unit, whereas the deterministic models reflect a significant change from small sand lenses within the clay till to an almost coherent sand deposit in the lowest part. The constant sizes in the TProGS model are caused by the use of the same transition probabilities throughout the entire unit. This was chosen under the assumption that the distribution was stationary within the unit. However, both the borehole and resistivity data illustrate a marked difference in the geological setting around 40 m above sea level. This underlines that it is difficult to obtain stationarity within geological environments − even at relatively small scales. Consequently, in the TProGS simulations, the sand lenses generally appear a little larger and more connected in the upper part of the unit and a little smaller and less connected in the lower part compared to the deterministic models. In both the TProGS simulations and in the MCG model, the sand lenses typically appear sloping, whereas most of the sand lenses in the CF model appear to be more horizontal. This is probably an artefact of the 2D search radius that is used in the interpolation of the translator function in the CF approach.

### 8.2. Quantitative evaluations

If we convert the MCG and the CF models into binary sand–clay models (Fig. 7a–b) and compare with a probability model based on 10 TProGS realisations, all of the models appear quite similar (compare Fig. 7a, b and c). To quantify this, analyses have been conducted for the binary models. The model outcomes are compared directly by deriving the number of cells where the models agree. To obtain identical grid dimensions all three model grids are resampled to 10 m × 10 m laterally and 2 m vertically. Also the quantification shows that the models are very much in agreement (82–84%). The agreement is slightly higher between the MCG model and the CF model (GM–CF: 84.6%) and the MCG model and the TProGS model (84.4%) compared to the CF and the TProGS model (CF–TProGS: 82.0%).

The mean sizes of the structures are considered by calculating transition probabilities of the model results (Fig. 8). The statistics in Fig. 8 represent the entire glacial unit, and therefore include both the small sand lenses within the clay till, and the bigger sand structures in the bottom of the unit. The transition probabilities show overall agreement between the models, but some minor variations, as slightly lower sand content in the TProGS model than in the deterministic models (Table 2). Thus, despite the very different methods in translating the resistivities to lithology, the sand proportions of Unit E fall in the same range for all the three models (23.7–25.6%). To investigate the difference between the statistics of the model results of the upper clay till sequence compared to the lower sandier sequence, transition probabilities have been calculated separately for the deterministic model results above and below 40 m a.s.l., respectively. The mean lengths derived from this analysis are in agreement with the visual inspection, since they show that the sand structures are considerably longer (2000 m for the MCG and 1200 m for the CF model) in this part of the model compared to the upper part (900 m for the MCG and 800 m for the CF model). Also, the sand proportions show that this part of the models contains considerably more sand than the upper part (74.2% for the MCG and 62.4% for the CF model). As witnessed in the visual inspection, the TProGS model shows the same mean lengths throughout the sequence. The vertical transition probabilities could not be calculated for the lower part of the sequence, because of too little data information.

**Table 2**
Sand proportions and length scales of the model results according to the transition probabilities. The results are shown for the entire Unit E, but also for the part of the Unit E that is above and below 40 m a.s.l. Note that there are 8 times more data located above 40 m a.s.l. than below.

|  | Sand proportion | Mean length of sand structures (horizontal) | Mean thickness of sand structures (vertical) |
| --- | --- | --- | --- |
| MCG (Unit E) | 25.3% | 900 m | 8 m |
| MCG (Unit E, above 40 m a.s.l.) | 19.3% | 900 m | 7 m |
| MCG (Unit E, below 40 m a.s.l.) | 74.2% | 2000 m | – |
| CF (Unit E) | 25.6% | 800 m | 10 m |
| CF (Unit E, above 40 m a.s.l.) | 20.7% | 800 m | 9 m |
| CF (Unit E, below 40 m a.s.l.) | 62.4% | 1200 m | – |
| TProGS model (Unit E) | 23.7% | 500 m | 5 m |

## 9. Discussion

Due to the overlap of resistivity intervals for different lithology types, it is a challenge to produce models with multiple lithological facies by using automated routines (Jørgensen et al., 2013). In our comparison, the MCG is the only model that enables incorporation of geological background knowledge. The most significant difference between the modelling methods is therefore that the two automated modelling methods deal with sand and clay, while the geological model operates with several lithological and stratigraphical units. The geological model therefore provides the highest degree of lithological and stratigraphic detail, but when transferred to binary models, all the models appear very similar (Figs. 7–8 and Table 2).

The outcome of the TProGS probability model closely reflects the input data, and the similarity between this and the two other models (in Unit E) emphasizes that they are all more or less data-dependent. The data density is high in the topmost part of the geological setting and data were highly weighted in all the modelling methods. At great depths, the significant differences between CF and MCG reflect the difference in the modelling methods. MCG takes the decrease in geophysical resolution and also the nature/limitations of geophysical inversion into account. In this study, we use smooth inversion of the data, which only allow for gradual changes in the resistivity models even though the geological setting contains sharp lithological boundaries (Høyer et al., 2014). In MCG, it is possible to include sharp sedimentary boundaries where such are expected. The CF method uses the inverted resistivity values directly and sharp layer boundaries are therefore not present in the model.

The different modelling methods require geological interpretations to different degrees. While deterministic geological modelling is completely based on geological interpretations, the stochastic simulations require geological pre-investigations to set up a conceptual geological framework model to help delineate model areas that represent relative stationarity. As witnessed in this study, however, it is difficult to find geological environments that represent true stationarity, and choosing such areas will therefore always represent a simplification of the geological environment. The CF method is less dependent on stationarity restrictions within the model area and it only requires a minimum of geological background knowledge in the form of realistic starting values for the translator function.

A challenge when working with 3D geological models is the evaluation of the uncertainty and credibility of the models. In MCG, the uncertainties cannot be estimated quantitatively, but can be subjectively estimated for each voxel under consideration of a number of factors. These include the credibility and resolution capabilities of the geophysical data, the quality of the borehole data and the uncertainty related to the geological interpretations. For the two other methods, measures for the uncertainty can be quantified on the basis of different assumptions. For the CF model, the calculated uncertainty is a function of the uncertainty of the boreholes and the AEM resistivity model. The TProGS method does not account for spatial variations in the geophysical model uncertainty, but allows for uncertainty estimation related to the geological variability through analysis of multiple realisations.

When quantifying the uncertainty, it is a problem to handle the borehole data that are qualitative in nature. Both the CF and the TProGS methods integrate the uncertainty via the borehole rating procedure, but the evaluation of the uncertainty related to each quality group is completely subjective. Furthermore, the methods are unable to include the uncertainties that cannot be described merely by a number, such as the uncertainty related to silt deposits erroneously interpreted as clay.

The different modelling methods are associated with their own strengths and limitations, and in general, the modelling objectives therefore need to guide the choice of the method. The MCG is the most time-consuming, but also the only one that provides stratigraphic and detailed lithological information. This method is therefore preferable when presenting the best estimate of the geological setting. For many years, MCG models have been used as basis for groundwater modelling in Denmark (Jørgensen et al., 2008). These models are typically simplified prior to hydrological modelling, but the detailed lithological and stratigraphical information are important when estimating porosities and hydraulic conductivities. Hence, the high degree of detail is often important during the groundwater modelling, since more geological information can be integrated if evaluated necessary. Also the CF model gives, to some degree, information regarding hydraulic conductivities through the multiple clay fraction categories, and preliminary results show that this method, when combined with clustering analysis, might provide useful models for groundwater modelling (Marker et al., 2014). However, it must be noted that the model outcome shows artefacts related to the nature of the geophysical inversion as, for instance, the gradual clay fraction changes across sharp layer boundaries. In areas with common findings of silty deposits, not well-described in the boreholes, the method is not preferable, because silt has relatively low hydraulic conductivities, but typically will appear as sand due to the high resistivities of the deposit.

The TProGS simulations provide a suite of realisations that can be difficult to handle in a traditional workflow, where the end-users normally require one, deterministic model. Nevertheless, the variance between the TProGS simulations is very useful for studying the uncertainty of the geological models, which are of great interest within the groundwater research (Beven and Binley, 1992; Delhomme, 1979; Feyen and Caers, 2006; Refsgaard et al., 2012). Also, the probability model can be very useful for various forecasts both within the groundwater research, but also for other applied geosciences (Stafleu et al., 2011). The individual stochastic simulations can be used as input for groundwater modelling, but the different positions of the structures will lead to considerably different travel path-ways and travel times (He et al., 2013). On the other hand, the estimation of the bulk hydraulic conductivity will benefit from the well-described connectivity in the stochastic models. Thus, studies have shown that the degree of connectivity of high permeability materials is crucial for controlling the groundwater flow and subsequent solute transport (Desbarats and Srivastava, 1991; Fogg, 1986; Silliman and Wright, 1988). In the TProGS simulations, the connectivity is indirectly defined through the estimated sand proportions and transition probabilities. As witnessed in our study, the connectivity of the small sand lenses in the clay till unit appears to be larger in the stochastic models than in the deterministic

models. The interconnectedness of this type of heterogeneities, not resolved by the data, is probably better simulated in the stochastic model than the deterministic models. The TProGS simulations can therefore contribute with valuable information for the groundwater modeller.

## 10. Conclusion

In this study we have compared three different modelling methods of AEM and borehole data with the objective to evaluate the ability of two automatic methods to resolve the geology and to provide realistic geological structures. It appears that the manually constructed geological model is the only one that provides stratigraphical information and also the only one that is able to inform about other sediment characteristics than just clay content. The CF modelling method is extremely time-efficient and provides a detailed lithological voxel model of clay fractions. Finally, the stochastic modelling provides a suite of equally plausible lithological realisations, which can be used to estimate uncertainty on for instance predictions from hydrological models. The modelling methods are highly different in nature and should be chosen to fit the later application of the model.

## Acknowledgements

## References

Auken, E., Christiansen, A.V., Westergaard, J.H., Kirkegaard, C., Foged, N., Viezzoli, A., 2009. An integrated processing scheme for high-resolution airborne electromagnetic surveys, the SkyTEM system. Explor. Geophys. 40 (2), 184–192.

Berg, C.B., Mathers, S.J., Kessler, H., Keefer, D.A., 2011. Synopsis of Current Three-dimensional Geological Mapping and Modeling in Geological Survey Organizations. Illinois State Geological Survey, Illinois.

Beven, K.J., Binley, A., 1992. The future of distributed models: model calibration and uncertainty prediction. Hydrol. Process. 6, 279–298.

Carle, S.F., 1999. T-PROGS: Transition Probability Geostatistical Software. USA University of California, Users Manual.

Carle, S.F., Fogg, G.E., 1996. Transition probability-based indicator geostatistics. Math. Geol. 28, 453–476.

Christiansen, A.V., Foged, N., Auken, E., 2014. A concept for calculating accumulated clay thickness from borehole lithological logs and resistivity models for nitrate vulnerability assessment. J. Appl. Geophys. 108, 69–77.

De Benedetto, D., Castrignano, A., Sollitto, D., Modugno, F., Buttafuoco, G., lo Papa, G., 2012. Integrating geophysical and geostatistical techniques to map the spatial variation of clay. Geoderma 171, 53–63.

Delhomme, J.P., 1979. Spatial variability and uncertainty in groundwater flow parameters: a geostatistical approach. Water Resour. Res. 15, 269–280.

Desbarats, A.J., Srivastava, R.M., 1991. Geostatistical characterization of groundwater flow parameters in a simulated aquifer. Water Resour. Res. 27 (5), 687–698.

Dybkjær, K., 2011a. Palynologisk undersøgelse af 1 prøve fra boringen DGU nr. 88.1559 (Solbjerg) og to prøver fra DGU nr. 98.1319 (Fillerup). De Nationale Geologiske Undersøgelser for Danmark og Grønland (GEUS).

Dybkjær, K., 2011b. Palynologisk undersøgelse af 4 prøver fra boringen DGU nr. 98.1315 ved Hovedgård, Østjylland. De Nationale Geologiske Undersøgelser for Danmark og Grønland (GEUS).

Engdahl, N.B., Weissmann, G.S., Bonal, N.D., 2010. An integrated approach to shallow aquifer characterization: combining geophysics and geostatistics. Comput. Geosci. 14 (2), 217–229.

Feyen, L., Caers, J., 2006. Quantifying geological uncertainty for flow and transport modeling in multi-modal heterogeneous formations. Adv. Water Resour. 29 (6), 912–929.

Foged, N., Marker, P.A., Christiansen, A.V., Bauer-Gottwein, P., Jørgensen, F., Høyer, A.-S., Auken, E., 2014. Large-scale 3-D modeling by integration of resistivity models and borehole data through inversion. Hydrol. Earth Syst. Sci. 18, 4349–4362.

Fogg, G.E., 1986. Groundwater flow and sand body interconnectedness in a thick multiple-aquifer system. Water Resour. Res. 22, 679–694.

Gunnink, J.L., Siemon, B., 2014. Applying airborne electromagnetics in 3D stochastic geohydrological modelling for determining groundwater protection. Near Surf. Geophys. 12.

Gunnink, J.L., Bosch, J.H.A., Siemon, B., Roth, B., Auken, E., 2012. Combining ground-based and airborne EM through Artificial Neural Networks for modelling glacial till under saline groundwater conditions. Hydrol. Earth Syst. Sci. 16, 3061–3074.

He, X., Sonnenborg, T.O., Jørgensen, F., Høyer, A.-S., Møller, R.R., Jensen, K.H., 2013. Analyzing the effects of geological and parameter uncertainty on prediction of groundwater head and travel time. Hydrol. Earth Syst. Sci. 10, 2789–2833.

He, X., Koch, J., Sonnenborg, T.O., Jørgensen, F., Schamper, C., Refsgaard, J.C., 2014a. Transition probability based stochastic geological modeling using airborne geophysical data and borehole data. Water Resour. Res. 50 (4), 3147–3169.

He, X.L., Sonnenborg, T.O., Jørgensen, F., Jensen, K.H., 2014b. The effect of training image and secondary data integration with multiple-point geostatistics in groundwater modelling. Hydrol. Earth Syst. Sci. Discuss. 18, 2943–2954.

Heilmann-Clausen, C., Nielsen, O.B., Gersner, P., 1985. Lithostratigraphy and depositional environments in the Upper Paleocene and Eocene of Denmark. Bull. Geol. Soc. Den. 33, 287–323.

Houmark-Nielsen, M., 1983. Glacial stratigraphy and morphology of the northern Bælthav region. In: Ehlers, J. (Ed.), Glacial Deposits in Northwest Europe Rotterdam. A A Balkema, pp. 199–202.

Houmark-Nielsen, M., 2011. Pleistocene glaciations in Denmark: a closer look at chronology, ice dynamics and landforms. In: Ehlers, J., Gibbard, P.L., Lughes, P.D. (Eds.), Quaternary Glaciations — Extent and Chronology. A Closer Look vol. 15. Elsevier, Developments in Quaternary Science, pp. 47–57.

Houmark-Nielsen, M., Berthelsen, A., 1981. Kineto-statigraphic evaluation and presentation of glacial–stratigraphic data, with examples from northern Samsø, Denmark. Boreas 10 (4), 411–422.

Høyer, A.-S., Møller, I., Jørgensen, F., 2013. Challenges in geophysical mapping of glaciotectonic structures. Geophysics 78 (5), B287–B303.

Høyer, A.-S., Jørgensen, F., Lykke-Andersen, H., Christiansen, A.V., 2014. Iterative modelling of AEM data based on a priori information from seismic and borehole data. Near Surf. Geophys. 12 (5), 635–650.

I-GIS, 2014. Geoscene3D: Aarhus, Denmark.

Jørgensen, F., Sandersen, P.B.E., 2006. Buried and open tunnel valleys in Denmark—erosion beneath multiple ice sheets. Quat. Sci. Rev. 25 (11–12), 1339–1363.

Jørgensen, F., Sandersen, P.B.E., Auken, E., 2003. Imaging buried Quaternary valleys using the transient electromagnetic method. J. Appl. Geophys. 53 (4), 199–213.

Jørgensen, F., Kristensen, M., Højbjerg, A.L., Klint, K.E.S., Hansen, C., Jordt, B.E., Richardt, N., Sandersen, P., 2008. Opstilling af geologiske modeller til grundvandsmodellering. Geo-Vejledning 3. Geological Survey of Denmark and Greenland (GEUS).

Jørgensen, F., Møller, R.R., Nebel, L., Jensen, N.-P., Christiansen, A.V., Sandersen, P.B.E., 2013. A method for cognitive 3D geological voxel modelling of AEM data. Bull. Eng. Geol. Environ. 72, 421–432.

Kessler, H., Mathers, S., Sobisch, H.-G., 2009. The capture and dissemination of integrated 3D geospatial knowledge at the British Geological Survey using GSI3D software and methodology. Comput. Geosci. 35, 1311–1321.

Koch, J., He, X., Jensen, K.H., Refsgaard, J.C., 2014. Challenges in conditioning a stochastic geological model of a heterogeneous glacial aquifer to a comprehensive soft data set. Hydrol. Earth Syst. Sci. 18, 2907–2923.

Larsen, G., Sand-Jensen, K., 2006. Naturen i Danmark: Geologien, Copenhagen, Gyldendal. Naturen i Danmark v. 1 (549 pp.).

Lee, S.Y., Carle, S.F., Fogg, G.E., 2007. Geologic heterogeneity and a comparison of two geostatistical models: sequential Gaussian and transition probability-based geostatistical simulation. Adv. Water Resour. 30 (no. 9), 1914–1932.

Marker, P.A., Foged, N., Christiansen, A.V., Mosegaard, K., Auken, E., Bauer-Gottwein, P., 2014. Informing regional groundwater models with airborne electromagnetic and borehole hydrostratigraphy. International Conference on Computational Methods in Water Resources (CMWR 2014).

Møller, I., Søndergaard, V.H., Jørgensen, F., Auken, E., Christiansen, A.V., 2009. Integrated management and utilization of hydrogeophysical data on a national scale. Near Surf. Geophys. 7 (5–6), 647–659.

Pedersen, S.A.S., Petersen, K.S., 1997. Djurslands geologi. National Survey of Denmark and Greenland, Copenhagen.

Rasmussen, E.S., Dybkjær, K., Piasecki, S., 2010. Lithostratigraphy of the Upper Oligocene–Miocene succession of Denmark. Geol. Surv. Den. Greenl. Bull. 22, 92–99 (plates).

Refsgaard, J.C., Christensen, S., Sonnenborg, T.O., Højbjerg, A.L., Troldborg, L., 2012. Review of strategies for handling geological uncertainty in groundwater flow and transport modeling. Adv. Water Resour. 36, 36–50.

Refsgaard, J.C., Auken, E., Bamberg, C.A., Christensen, B.S.B., Clausen, T., Dalgaard, E., Effersø, F., Ernstsen, V., Gertz, F., Hansen, A.L., He, X., Jacobsen, B.H., Jensen, K.H., Jørgensen, F., Jørgensen, L.F., Koch, J., Nilsson, B., Petersen, C., Schepper, G.D., Schamper, C., Sørensen, K.I., Therrien, R., Thirup, C., Viezzoli, A., 2014. Nitrate reduction in geologically heterogeneous catchments — a framework for assessing the scale of predictive capability of hydrological models. Sci. Total Environ. 468–469, 1278–1288.

Royse, K.R., 2010. Combining numerical and cognitive 3D modelling approaches in order to determine the structure of the Chalk in the London Basin. Comput. Geosci. 36, 500–511.

Schamper, C., Auken, E., Sørensen, K.I., 2012. A new processing system for very early time SkyTEM101 data. 22nd International Geophysical Conference & Exhibition, ASEG 26–29 February 2012: Brisbane, Australia.

Schamper, C., Jørgensen, F., Auken, E., Effersø, F., 2014. Assessment of near-surface mapping capabilities by airborne transient electromagnetic data—an extensive comparison to conventional borehole data. Geophysics 79 (4), B187–B199.

Siemon, B., Christiansen, A.V., Auken, E., 2009. A review of helicopter-borne electromagnetic methods for groundwater exploration. Near Surf. Geophys. 7 (5–6), 629–646.

Silliman, S.E., Wright, A.L., 1988. Stochastic analysis of paths of high hydraulic conductivity in porous media. Water Resour. Res. 24 (11), 1901–1910.

Sørensen, K.I., Auken, E., 2004. SkyTEM — a new high-resolution helicopter transient electromagnetic system. Explor. Geophys. 35 (3), 191–199.

Stafleu, J., Maljers, D., Gunnink, J.L., Menkovic, A., Busschers, F.S., 2011. 3D modelling of the shallow subsurface of Zeeland, the Netherlands. Neth. J. Geosci. — Geol. Mijnb. 90 (4), 293–310.

Strebelle, S.B., 2002. Conditional simulation of complex geological structures using multiple-point statistics. Math. Geol. 34 (1), 1–21.

Turner, A.K., 2006. Challenges and trends for geological modelling and visualisation. Bull. Eng. Geol. Environ. 65, 109–127.

Van der Meulen, M.J., Doornenbal, J.C., Gunnink, J.L., Stafleu, J., Schokker, J., Vernes, R.W., Van Geer, F.C., Van Gessel, S.F., Van Heteren, S., Van Leeuwen, R.J.W., Bakker, M.A.J., Bogaard, P.J.F., Busschers, F.S., Griffioen, J., Gruijters, S.H.L.L., Kiden, P., Schroot, B.M., Simmelink, H.J., Van Berkel, W.O., Van der Krogt, R.A.A., Westerhoff, W.E., Van Daalen, T.M., 2013. 3D geology in a 2D country: perspectives for geological surveying in the Netherlands. Neth. J. Geosci. 92 (4), 217–241.

Viezzoli, A., Christiansen, A.V., Auken, E., Sørensen, K., 2008. Quasi-3D modeling of airborne TEM data by spatially constrained inversion. Geophysics 73 (3), F105–F113.

Wycisk, P., Hubert, T., Gossel, W., Neumann, C., 2009. High-resolution 3D spatial modelling of complex geological structures for an environmental risk assessment of abundant mining and industrial megasites. Comput. Geosci. 35, 165–182.